

Primordial black holes and induced gravitational waves in Galileon inflation

Milad Solbi* and Kayoomars Karami†

*Department of Physics, University of Kurdistan,
Pasdaran Street, P.O. Box 66177-15175, Sanandaj, Iran*

(Dated: December 23, 2024)

Abstract

Recent observational constraints indicate that primordial black holes (PBHs) with the mass scale $\sim 10^{-12}M_{\odot}$ can explain most of dark matter in the Universe. To produce this kind of PBHs, we need an enhance in the primordial scalar curvature perturbations to the order of $\mathcal{O}(10^{-2})$ at the scale $k \sim 10^{12} \text{ Mpc}^{-1}$. Here, we investigate the production of PBHs and induced gravitational waves (GWs) in the framework of Galileon inflation. To this aim, we consider the Galileon term $G(X) = X/M^3$ as well as the α -attractor base potential modified by a small local Gaussian bump. We solve numerically the Mukhanov-Sasaki equation to obtain the primordial scalar power spectrum. In addition, we estimate the PBHs abundance $f_{\text{PBH}}^{\text{peak}}$ as well as the energy density parameter $\Omega_{\text{GW},0}$ of induced GWs. Interestingly enough is that for a special set of model parameters, we estimate the mass scale and the abundance of PBHs as $\sim \mathcal{O}(10^{-12})M_{\odot}$ and $f_{\text{PBH}}^{\text{peak}} = 0.92$, respectively. This confirms that the mechanism of PBHs production in Galileon inflation can justify most of dark matter. Furthermore, we evaluate the GWs energy density parameter and conclude that it behaves like a power-law function $\Omega_{\text{GW}} \sim (f/f_c)^n$ where in the infrared limit $f \ll f_c$, the power index reads $n = 3 - 2/\ln(f_c/f)$.

PACS numbers:

* miladsolbi@gmail.com

† kkarami@uok.ac.ir

I. INTRODUCTION

Primordial black holes (PBHs) have been a topic of debate for years [1–3]. The existence of PBHs was proposed by Zel’dovich and Novikov for the first time in 1967 [4]. PBHs received new attentions after the LIGO-Virgo team detected gravitational waves (GWs) from a binary black hole (BH). After the first detection, the LIGO-Virgo collaboration observed some of these GW events from binary BHs [5–9]. They found that the mass of these BHs is nearly $30M_{\odot}$. The stellar BHs do not fall on this mass scale. However, PBHs that have a wide mass range can explain this type of BHs. In other words, PBHs can be a candidate for the origin of BHs that was discovered by LIGO-Virgo collaboration [10–13].

PBHs with a $12\text{--}213\text{ Gpc}^{-3}\text{yr}^{-1}$ merger rate and mass about $10M_{\odot}$ have good consistency with the LIGO-Virgo observations [7]. Sasaki et al. [12] showed that PBHs with this merger rate can constitute approximately $\mathcal{O}(1)\%$ of the total dark matter (DM). Recently in the OGLE data, six microlensing events were detected, which have ultra-short timescales [14]. The results of this investigation show that PBHs with a mass scale of $\mathcal{O}(10^{-5})M_{\odot}$ and the abundance around $\mathcal{O}(10^{-2})$ can locate in the allowed region of OGLE data [14].

Following the recent observations of white dwarf explosion (WD) [15] and microlensing events with Subaru HSC (Subaru HSC) [16, 17], it is possible that the PBHs with the mass range $\mathcal{O}(10^{-13})M_{\odot} \leq M \leq \mathcal{O}(10^{-11})M_{\odot}$ can describe all DM.

The collapse of primordial curvature perturbations after horizon reentry can form PBHs. For PBHs production, the amplitude of primordial curvature perturbations needs to be increased by nearly seven orders to $A_s \sim \mathcal{O}(10^{-2})$ [18]. At the pivot scale $k_* = 0.05\text{Mpc}^{-1}$, the exact value of the primordial curvature perturbations has been estimated by cosmic microwave background (CMB) observations. The CMB anisotropy measurements show $A_s = 2.1 \times 10^{-9}$ [19]. The enhancement of the curvature perturbations leads to an overdense region. After horizon reentry, these overdense areas can generate considerable metric perturbations in addition to PBHs. In contrary to the linear level, scalar and tensor perturbation couplings occur at the second order. The scalar metric perturbations can produce the stochastic GW background through the second-order effect [20–29]. Hence, induced GWs signal detection suggests a new way of looking for the existence of PBHs.

More recently, in the context of inflation, different mechanisms of PBHs production have been proposed, see e.g. [30–45]. For instance, in the single field model of inflation with a

potential containing an inflection point, the primordial curvature power spectrum can be enhanced at small scales [34–36]. Indeed, in the vicinity of inflection point, the inflaton experiences the ultra slow-roll (USR) phase. Then, the inflaton velocity decreases in the USR phase due to high friction and curvature perturbation increases consequently. On the other hand, Mishra et al. [45] proposed an alternative method for increasing curvature perturbations. They used a small local bump-like feature in the base potential of inflation. Based on their results, the amplitude of curvature perturbations severely enhances due to the local bump.

In the context of inflation, the Galileon scalar field scenario is one of the most attractive models [46]. The Galileon inflation takes place in a sub-class of the Horndeski theory [47]. Hirano et al. [48] pointed out that Galileon inflation models can explain CMB anomalies when the inflaton goes into the USR phase. Also, they showed that the Galileon inflation in the USR phase can illustrate the decaying of CMB power spectrum at the largest scales.

In this paper, we investigate the possibility of PBH formation in the Galileon scenario when the base inflationary potential is α -attractor perturbed by a small local bump. The outline of the paper is as follows. We review Galileon inflation in Sec. II. The mechanism of PBH formation is explained in Sec. III. In Sec. IV, we calculate the abundance of PBHs. The induced GWs are studied in Sec. V. Also Sec. VI is devoted to our conclusions.

II. GALILEON INFLATION

The general action of Galileon inflation is given by [46]

$$S = \int d^4x \sqrt{-g} \left[\frac{M_{\text{pl}}^2}{2} R + \mathcal{L}_\phi \right], \quad (1)$$

where

$$\mathcal{L}_\phi \equiv K(\phi, X) - G(\phi, X) \square \phi, \quad (2)$$

is the Lagrangian of the scalar field, and g and R are the determinant of the metric $g_{\mu\nu}$ and Ricci scalar, respectively. Also K and G are the general functions of the scalar field ϕ and the kinetic term $X \equiv -\frac{1}{2}g^{\mu\nu}\phi_{,\mu}\phi_{,\nu}$.

In the framework of Galileon gravity (1), the Friedmann equations take the forms [46, 49]

$$3M_{\text{pl}}^2 H^2 = 2K_{,X}X - K + 3G_{,X}H\dot{\phi}^3 - 2G_{,\phi}X, \quad (3)$$

$$-M_{\text{pl}}^2 \left(3H^2 + 2\dot{H} \right) = K - 2 \left(G_{,\phi} + G_{,X}\ddot{\phi} \right) X, \quad (4)$$

where $_{,X} \equiv d/dX$ and $_{,\phi} \equiv d/d\phi$. Also the dot denotes the derivative with respect to the cosmic time. The scalar field equation of motion from action (1) can be derived as

$$\begin{aligned} K_{,X} \left(\ddot{\phi} + 3H\dot{\phi} \right) + 2K_{,XX}X\ddot{\phi} + 2K_{,X\phi}X - K_{,\phi} - 2 \left(G_{,\phi} - G_{,X\phi}X \right) \left(\ddot{\phi} + 3H\dot{\phi} \right) \\ + 6G_{,X} \left[(HX) \cdot + 3H^2X \right] - 4G_{,X\phi}X\ddot{\phi} - 2G_{,\phi\phi}X + 6HG_{,XX}X\dot{X} = 0. \end{aligned} \quad (5)$$

The second order action for curvature perturbation \mathcal{R} at the first order approximation is found to be [46]

$$S^{(2)} = \frac{1}{2} \int d\tau d^3x z^2 \left[\mathcal{G}(\mathcal{R}'_{\phi})^2 - \mathcal{F}(\vec{\nabla}\mathcal{R}_{\phi})^2 \right], \quad (6)$$

in which

$$z \equiv \frac{a\dot{\phi}}{H - G_{,X}\dot{\phi}^3/2M_{\text{pl}}^2}, \quad (7)$$

$$\mathcal{F} \equiv K_{,X} + 2G_{,X} \left(\ddot{\phi} + 2H\dot{\phi} \right) - 2\frac{G_{,X}^2}{M_{\text{pl}}^2}X^2 + 2G_{,XX}X\ddot{\phi} - 2 \left(G_{,\phi} - XG_{,\phi X} \right), \quad (8)$$

$$\mathcal{G} \equiv K_{,X} + 2XK_{,XX} + 6G_{,X}H\dot{\phi} + 6\frac{G_{,X}^2}{M_{\text{pl}}^2}X^2 - 2 \left(G_{,\phi} + XG_{,\phi X} \right) + 6G_{,XX}HX\dot{\phi}, \quad (9)$$

and the prime shows the derivative with respect to the conformal time τ . According to [46], the squared sound speed is obtained as $c_s^2 = \mathcal{F}/\mathcal{G}$, where the conditions $\mathcal{F} > 0$ and $\mathcal{G} > 0$ are needed to avoid of ghost and gradient instability.

The power spectrum of \mathcal{R} produced during the Galileon inflation can be assessed in the Fourier space by writing the Mukhanov-Sasaki (MS) equation as

$$\frac{d^2 u_k}{dy^2} + \left(k^2 - \frac{\tilde{z}_{,yy}}{\tilde{z}} \right) u_k = 0, \quad (10)$$

where $dy = c_s d\tau$, $\tilde{z} \equiv (\mathcal{F}\mathcal{G})^{1/4} z$, and $u_k \equiv \tilde{z}\mathcal{R}_{\phi,k}$ [46]. Also the scalar power spectrum is given by

$$\mathcal{P}_{\mathcal{R}}(k) = (2\pi^2)^{-1} k^3 |u_k/z|^2. \quad (11)$$

Hereafter in the Lagrangian (2), we take

$$K(\phi, X) = X - V(\phi). \quad (12)$$

Also following [49–52], we assume that G depends only on X and is given by

$$G(X) = X/M^3, \quad (13)$$

in which M is a constant with mass dimension.

Now, we are interested in investigating the Galileon inflation in the slow-roll regime. In the slow-roll approximation $\varepsilon \equiv -\dot{H}/H^2 \ll 1$ and $\eta \equiv -\ddot{\phi}/(H\dot{\phi}) \ll 1$, one can easily show that the background Eqs. (3) and (5) are simplified into [49, 52]

$$3M_{\text{pl}}^2 H^2 \simeq V(\phi), \quad (14)$$

$$3H\dot{\phi}(1 + \mathcal{D}) + V_{,\phi} \simeq 0, \quad (15)$$

where

$$\mathcal{D}(\phi) = \frac{1}{2} \left(\sqrt{1 - \frac{4V_{,\phi}}{M^3}} - 1 \right). \quad (16)$$

In the slow-roll regime, the power spectrum of curvature perturbations and primordial gravitational waves are given by [49, 52]

$$\mathcal{P}_{\mathcal{R}} \simeq \frac{1}{12 \pi^2 M_{\text{pl}}^6} \left(\frac{V^3}{V_{,\phi}^2} \right) \frac{(1 + \mathcal{D})^2 (1 + 2\mathcal{D})^{1/2}}{(1 + 4\mathcal{D}/3)^{3/2}}, \quad (17)$$

and

$$\mathcal{P}_T = \frac{2H^2}{\pi^2 M_{\text{pl}}^2} \simeq \frac{2V(\phi)}{3\pi^2 M_{\text{pl}}^4}, \quad (18)$$

respectively. Consequently, the scalar spectral index and the tensor-to-scalar ratio can be obtained as

$$n_s - 1 = -\frac{6\varepsilon_v}{1 + \mathcal{D}} + \frac{2\eta_v}{1 + 4\mathcal{D}/3} \left[1 - \frac{\mathcal{D}}{6(1 + 2\mathcal{D})^2} \right], \quad (19)$$

$$r = 16\varepsilon_v \frac{(1 + 4\mathcal{D}/3)^{3/2}}{(1 + \mathcal{D})^2 (1 + 2\mathcal{D})^{1/2}}, \quad (20)$$

where $\varepsilon_v \equiv \frac{M_{\text{pl}}^2}{2} \left(\frac{V_{,\phi}}{V} \right)^2$ and $\eta_v \equiv M_{\text{pl}}^2 \frac{V_{,\phi\phi}}{V}$ are defined as potential slow-roll parameters. In the next section, we present the results of exact numerical solutions obtained for the background equations (3), (5) as well as the MS equation (10). We use the slow-roll solutions as initial conditions for our numerical calculations.

III. PBH FORMATION MECHANISM

In the method proposed by Mishra et al. [45], a small local bump adds to the base potential of inflation. The small bump generates a significant increase in the amplitude of the curvature spectrum. A significant example of a local speed breaker occurs when a term

such as $V_b(\phi)\gamma(\phi)$ where $\gamma(\phi) \ll 1$, located at ϕ_0 is attached to the base inflation potential of $V_b(\phi)$. Following [45], the general form of potential is given by

$$V(\phi) = V_b(\phi) \left[1 + \gamma(\phi) \right], \quad (21)$$

where $V_b(\phi)$ is the base potential of inflation that is responsible for producing quantum fluctuations consistent with the CMB constraints on n_s and r . The quantity $\gamma(\phi)$ defines the bump in the potential. It is necessary that the base potential leads to $0.956 \leq n_s \leq 0.978$. Under this condition, the CMB bound on n_s is verified, while the scalar curvature successfully increases to generate PBHs at a small scale.

In the present work, like [45] we consider the α -attractor potential as the base potential which is given by

$$V_b(\phi) = V_0 \tanh^2 \left(\frac{\phi}{\sqrt{6\alpha}M_{\text{pl}}} \right), \quad (22)$$

where V_0 is fixed by $P_{\mathcal{R}}(k_*) = 2.1 \times 10^{-9}$ and $k_* = 0.05 \text{ Mpc}^{-1}$ denotes the pivot scale. Also, we take a Gaussian form for the local bump in (21) as

$$\gamma(\phi) = A \exp \left(-\frac{1}{2} \frac{(\phi - \phi_c)^2}{\sigma^2} \right), \quad (23)$$

where A , ϕ_c and σ determine the height, position and width of the bump, respectively.

Therefore, our model is characterized by a set of six parameters (i.e. α , V_0 , A , σ , ϕ_c , and M). We set $N_* = 0$ at the horizon exit and take the slow-roll value for the scalar field as $\phi_* \simeq 6$ at the pivot scale $k_* = 0.05 \text{ Mpc}^{-1}$. We further consider $\alpha = 1$ and $M = 10^{-3}$, which lead to $n_s \simeq 0.966$ and $r \simeq 0.0039$ and can satisfy the CMB bounds on n_s and r . Moreover, the parameter V_0 is fixed by the power spectrum at the CMB scale. Therefore, A , σ , and ϕ_c are the only remaining parameters in our model which can affect scalar perturbation evolution and PBH production.

Note that beyond the slow-roll conditions, Eq. (17) does not hold and we need to solve the MS equation (10) numerically to obtain the scalar power spectrum $\mathcal{P}_{\mathcal{R}}(k) = (2\pi^2)^{-1} k^3 |u_k/z|^2$. To do this, for the three sets of parameters listed in Table I we could find the corresponding power spectrum with suitable enhance in PBH production. In Fig. 1(a), evolution of the scalar field versus the e -fold number is presented for the parameter set C. The flat part in Fig. 1(a) is due to the addition of a local bump in the base potential where the slow-roll condition is violated and inflaton is passing the USR phase. Hence, the

scalar curvature perturbations intensively enhance. As shown in Fig. 1(b), the value of η becomes larger than 1, and the slow-roll condition is not respected. The sharp decrease in ϵ can provide considerably increase in the scalar power spectrum.

TABLE I: The selected parameter sets for PBHs production

Sets	ϕ_c	A	σ	$k_{\text{peak}}/\text{Mpc}^{-1}$	$M_{\text{PBH}}^{\text{peak}}/M_{\odot}$	$\mathcal{P}_{\mathcal{R}}^{\text{peak}}$	$f_{\text{PBH}}^{\text{peak}}$
A	5.64	5.2369×10^{-4}	9.501×10^{-3}	3.11×10^5	29.1	0.061	0.0022
B	5.38	7.4147×10^{-4}	1.0705×10^{-2}	3.94×10^8	1.8×10^{-5}	0.051	0.021
C	5	1.4344×10^{-3}	1.5435×10^{-2}	1.42×10^{12}	1.38×10^{-12}	0.042	0.92

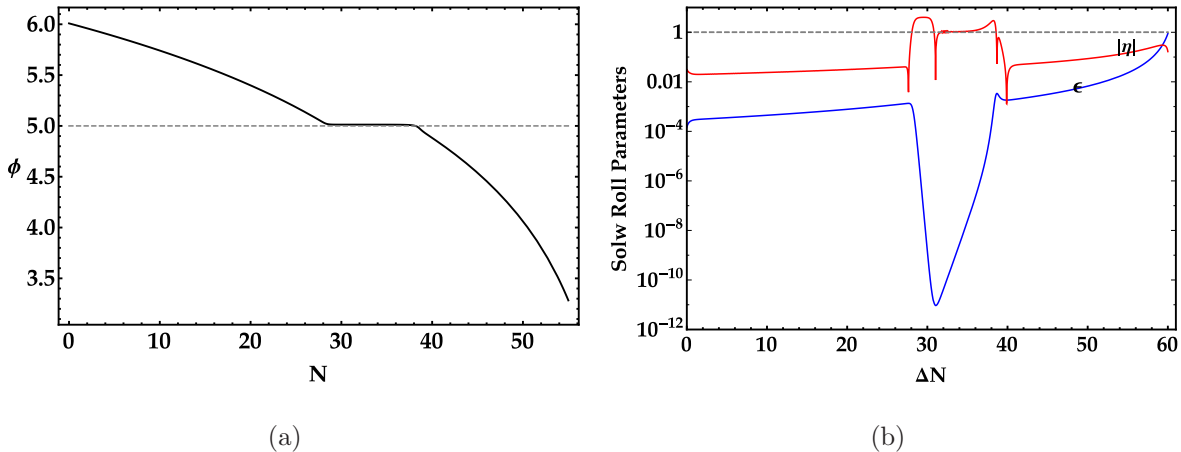


FIG. 1: (a) Evolution of the scalar field ϕ versus the e -fold number N . The dashed line represents $\phi = \phi_c$. (b) Evolution of the slow-roll parameters ϵ and η in terms of N . The dashed line shows the violation of the slow-roll condition. The auxiliary parameters are given by the parameter set C in Table I and we take $N_* = 0$ at the horizon exit.

In Fig. 2, the scalar power spectrum is plotted for the all parameter sets listed in Table I. The results show that at the CMB scale (i.e. $k \sim 0.05 \text{ Mpc}^{-1}$), the power spectrum is in order of $\mathcal{O}(10^{-9})$ which is consistent with the observations. Figure presents that the PBHs are generated when the peak of the scalar power spectrum increases by nearly seven orders of magnitudes, i.e. $\mathcal{P}_{\mathcal{R}}^{\text{peak}} \sim \mathcal{O}(10^{-2})$, at small scales. Our result for the PBHs production is in well agreement with the constraints deduced from the observations of CMB μ -distortion, big bang nucleosynthesis (BBN), and pulsar timing array (PTA) [53–55].

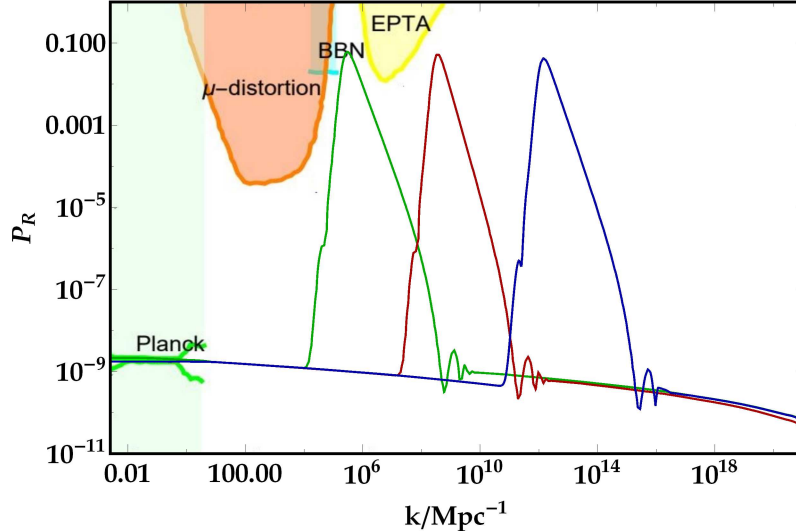


FIG. 2: The scalar power spectrum $\mathcal{P}_{\mathcal{R}}$ in terms of wavenumber k . The green, red and blue lines are corresponding to the parameter sets A , B and C , respectively. The CMB observations exclude the light-green shaded area [19]. The yellow region demonstrates the constraint from the PTA observations [53]. The cyan area represents the effect on the ratio between neutron and proton during the big bang nucleosynthesis (BBN) [54]. The orange zone shows the μ -distortion of CMB [55].

IV. ABUNDANCE OF PRIMORDIAL BLACK HOLES

Here, we are interested in obtaining the abundance of PBHs. In [56], it was shown that the primordial curvature perturbations re-enter the horizon during the radiation-dominated (RD) era. If primordial curvature perturbations undergo a significant rise, the gravity of this overdense region can overcome the RD pressure at the horizon re-entry. Consequently, the collapse of curvature perturbations can produce PBHs.

The PBH mass at the production time is given by $M = \gamma M_{\text{H}}$, where M_{H} is the horizon mass [57–64]. Also the parameter γ indicates the collapse efficiency, which relies on the characteristics of gravitational collapse. In this paper, we consider $\gamma = 0.2$ [3, 57, 65]. The ratio of the PBH mass to the total DM at the present time is given by [57]

$$f_{\text{PBH}}(M_{\text{PBH}}) = 1.68 \times 10^8 \left(\frac{\gamma}{0.2}\right)^{\frac{1}{2}} \left(\frac{g_*}{106.75}\right)^{-\frac{1}{4}} \left(\frac{M_{\text{PBH}}}{M_{\odot}}\right)^{-\frac{1}{2}} \beta(M_{\text{PBH}}), \quad (24)$$

where g_* indicates the effective degrees of freedom in the energy density during the PBH production process. Following [34], we take $g_* = 106.75$ to form the PBHs in the RD era.

Also, β is the mass fraction of PBH and can be calculated by [57, 66, 67]

$$\beta(M_{\text{PBH}}) = \gamma \frac{\sigma_{M_{\text{PBH}}}}{\sqrt{2\pi}\delta_{\text{th}}} \exp\left(-\frac{\delta_{\text{th}}^2}{2\sigma_{M_{\text{PBH}}}^2}\right), \quad (25)$$

where δ_{th} is the threshold density contrast for PBH production. Many studies indicate that the numerically-approved threshold value may be very wide, with δ_{th} ranging from 0.3 to 0.66 for PBH formation in the RD era [67–72]. In the present work, we set $\delta_{\text{th}} = 0.4$, which is consistent with the calculations in Refs. [67, 68].

Furthermore, $\sigma_{M_{\text{PBH}}}$ in Eq. (25) stands for the variance of density contrast at the comoving horizon scale. The value of $\sigma_{M_{\text{PBH}}}$ is dependent on the mass of PBH $M(k)$ and is obtained as [66]

$$\sigma_k^2 = \left(\frac{4}{9}\right)^2 \int \frac{dq}{q} W^2(q/k) (q/k)^4 P_{\mathcal{R}}(q), \quad (26)$$

where $W(x) = \exp(-x^2/2)$ is the Gaussian windows function. The mass of PBHs and the associated wavenumber can be related as [34, 45, 57]

$$M_{\text{PBH}} = 1.13 \times 10^{15} \left(\frac{\gamma}{0.2}\right) \left(\frac{g_*}{106.75}\right)^{-\frac{1}{6}} \left(\frac{k_{\text{PBH}}}{k_*}\right)^{-2} M_{\odot}. \quad (27)$$

The abundance of PBHs for each set of parameters in Table I can be calculated using Eqs. (24) and (27). The results are displayed in Fig. 3. The shaded areas indicate the observational constraints on the PBH abundance. Figure 3 shows that: (i) For the parameter set A, the peak of the PBH abundance is located at $29.1M_{\odot}$ and its value is approximately $f_{\text{PBH}}^{\text{peak}} \sim 0.0022$. The achieved result for this case can describe the LIGO events, and it is compatible with the upper limit bounds on the LIGO merger rate. (ii) For the case B, the abundance peak occurs at $M_{\text{PBH}}^{\text{peak}} = 1.8 \times 10^{-5}M_{\odot}$ and the mass spectrum height rises to 0.021 which is located at the allowed region of microlensing events in the OGLE data. (iii) Interestingly enough is that for the set C, we obtain the mass scale for the PBHs as $\sim \mathcal{O}(10^{-12})M_{\odot}$ which lies in the observational region $\mathcal{O}(10^{-13})M_{\odot} \leq M \leq \mathcal{O}(10^{-11})M_{\odot}$. Besides, we estimate the PBHs abundance as $f_{\text{PBH}}^{\text{peak}} = 0.92$ which indicates the mechanism of the PBHs production can justify the most of DM in the Universe.

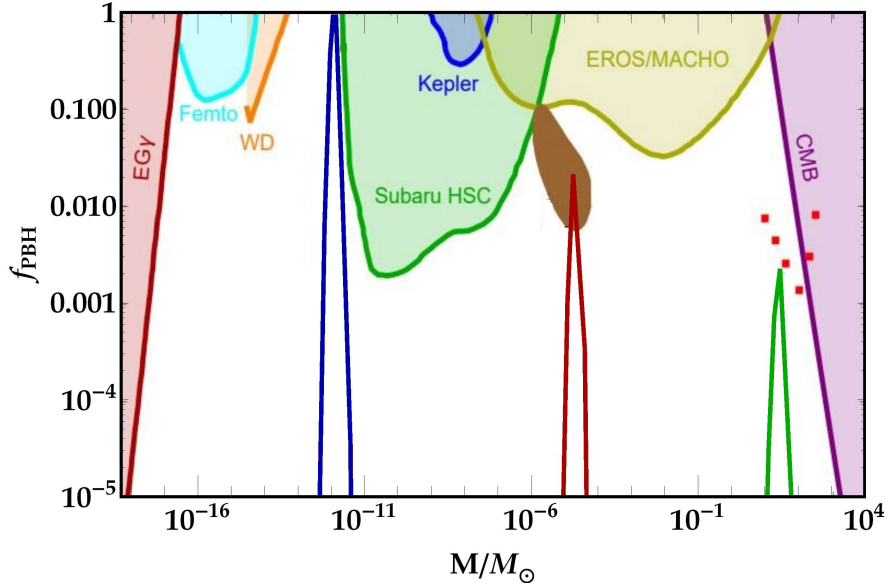


FIG. 3: The PBHs abundance f_{PBH} for the parameter sets A (green line), B (red line), and C (blue line). The observational constraints on PBH abundance are shown by the shaded areas. The red dots show the upper bound on the PBH abundance due to the upper limit on the LIGO event merger rate [73]. The brown shaded area shows the allowed region of PBH abundance in the OGLE data [14]. Other shaded regions illustrate the recent observational constraints including extragalactic gamma rays from PBH evaporation (EG γ) [74], femtolensing of gamma-ray burst (Femto) [75], white dwarf explosion (WD) [15], microlensing events with Subaru HSC (Subaru HSC) [16, 17], with the Kepler satellite (Kepler) [76], with EROS/MACHO (EROS/MACHO) [77], and accretion constraints from CMB [78, 79].

V. INDUCED GRAVITATIONAL WAVES

The induced GWs can form simultaneously with PBHs when the large density disturbances re-enter the horizon in the RD era [20–29]. The induced GWs can be tested by the future observations of PTA [80–83] and space-based GWs observatory, such as LISA [84]. In the conformal Newtonian gauge, the perturbed Friedmann-Robertson-Walker (FRW) metric has the following form [85]

$$ds^2 = a(\eta)^2 \left\{ -(1 + 2\Psi)d\eta^2 + \left[(1 - 2\Psi)\delta_{ij} + \frac{h_{ij}}{2} \right] dx^i dx^j \right\}, \quad (28)$$

where a and η represent the scale factor and conformal time, respectively. Also Ψ is the first-order scalar perturbations, and h_{ij} denotes the perturbation of the second-order transverse-

traceless tensor. The inflaton would decay into light particles after the inflation to thermalize our universe once the reheating is over. Hence, the effect of the inflaton field is ignorable. Consequently, the standard Einstein equation will work properly during RD. Therefore, the second-order tensor perturbations h_{ij} satisfy [85, 86]

$$h''_{ij} + 2\mathcal{H}h'_{ij} - \nabla^2 h_{ij} = -4\mathcal{T}_{ij}^{lm} S_{lm} , \quad (29)$$

where $\mathcal{H} \equiv a'/a$ is the conformal Hubble parameter, and the quantity \mathcal{T}_{ij}^{lm} is described as the transverse-traceless projection operator. The GW source term S_{ij} is given by

$$S_{ij} = 4\Psi\partial_i\partial_j\Psi + 2\partial_i\Psi\partial_j\Psi - \frac{1}{\mathcal{H}^2}\partial_i(\mathcal{H}\Psi + \Psi')\partial_j(\mathcal{H}\Psi + \Psi') . \quad (30)$$

The scalar metric perturbation Ψ in the RD takes the form [86]

$$\Psi_k(\eta) = \psi_k \frac{9}{(k\eta)^2} \left(\frac{\sin(k\eta/\sqrt{3})}{k\eta/\sqrt{3}} - \cos(k\eta/\sqrt{3}) \right) , \quad (31)$$

where k is the comoving wavenumber, and the primordial perturbation ψ_k is obtained as

$$\langle \psi_{\mathbf{k}} \psi_{\tilde{\mathbf{k}}} \rangle = \frac{2\pi^2}{k^3} \left(\frac{4}{9} \mathcal{P}_{\mathcal{R}}(k) \right) \delta(\mathbf{k} + \tilde{\mathbf{k}}) . \quad (32)$$

In the RD era, the energy density of induced GWs reads [20]

$$\begin{aligned} \Omega_{\text{GW}}(\eta_c, k) &= \frac{1}{12} \int_0^\infty dv \int_{|1-v|}^{|1+v|} du \left(\frac{4v^2 - (1+v^2 - u^2)^2}{4uv} \right)^2 \mathcal{P}_{\mathcal{R}}(ku) \mathcal{P}_{\mathcal{R}}(kv) \left(\frac{3}{4u^3 v^3} \right)^2 (u^2 + v^2 - 3)^2 \\ &\times \left\{ \left[-4uv + (u^2 + v^2 - 3) \ln \left| \frac{3 - (u+v)^2}{3 - (u-v)^2} \right| \right]^2 + \pi^2 (u^2 + v^2 - 3)^2 \Theta(v + u - \sqrt{3}) \right\} , \quad (33) \end{aligned}$$

where Θ denotes the Heaviside theta function, and η_c represents the time when Ω_{GW} stops to grow. The energy spectra of the induced GWs at the present time is given by [53]

$$\Omega_{\text{GW},0} h^2 = 0.83 \left(\frac{g_c}{10.75} \right)^{-1/3} \Omega_{\text{r},0} h^2 \Omega_{\text{GW}}(\eta_c, k) , \quad (34)$$

where $\Omega_{\text{r},0} h^2 \simeq 4.2 \times 10^{-5}$ is the current radiation density parameter, while $g_c \simeq 106.75$ is the effective degrees of freedom in the energy density at η_c . The frequency and wavenumber can be converted to each other as

$$f = 1.546 \times 10^{-15} \frac{k}{1 \text{Mpc}^{-1}} \text{Hz} . \quad (35)$$

Now, the current energy density of the induced GWs can be obtained from Eqs. (33) to (35) and using the power spectrum estimated by the MS equation (10).

In Fig. 4, the numerical results obtained for $\Omega_{\text{GW},0}$ are illustrated. Figure 4 shows that the induced GWs fall in the mHz band for the parameter set C and can be examined by the space-based observatories, such as LISA, Taiji, and TianQin. The induced GWs generated from the parameter sets A and B have peaks in frequencies $f \sim 10^{-10}\text{Hz}$ and $f \sim 10^{-7}\text{Hz}$, respectively, and both of them can be tested by the SKA observation.

The energy density of induced GWs can be modeled by a power-law function of frequency $\Omega_{\text{GW}}(f) \sim f^n$ [27, 87]. This parametrization can be considered as a powerful tool in probing history of the universe [88]. For the parameter set C , we obtain $\Omega_{\text{GW}} \sim f^{2.1}$ for $f < f_c = 3.62 \times 10^{-3}\text{Hz}$, and $\Omega_{\text{GW}} \sim f^{-3.36}$ for $f > f_c$. In the infrared limit $f \ll f_c$, the power index is determined as $n = 3 - 2/\ln(f_c/f)$, which is completely consistent with the analytical result obtained in [89].

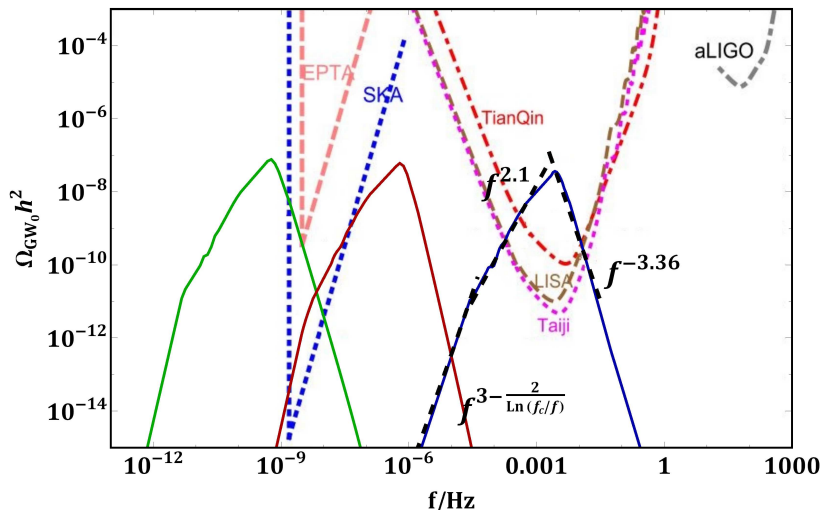


FIG. 4: The induced GWs energy density parameter $\Omega_{\text{GW},0}$ produced from the parameter sets A (green line), B (red line), and C (blue line). The broken power-law behaviour of Ω_{GW} is shown by black dashed line. The dashed curves indicate sensitivity of GWs observatories, such as the European PTA (EPTA) [80–83], the Square Kilometer Array (SKA) [90], the Advanced Laser Interferometer Gravitational Wave Observatory (aLIGO) [91, 92], the Laser Interferometer Space Antenna (LISA) [84, 93], Taiji [94] and TianQin [95].

VI. CONCLUSIONS

Here, we investigated the production of primordial black holes in Galileon inflation when the inflationary potential is perturbed by a tiny local bump. The base potential is the α -attractor, and the local bump has a Gaussian form. A flat plateau is generated during

evolution of the scalar field due to local bump perturbation. In this region, the scalar field enters the USR regime when the slow-roll condition is violated. Consequently, the primordial scalar curvature perturbations can increase in the USR phase and form PBHs. Our results show an increase in the scalar power spectrum to order 10^{-2} , which is sufficient for PBH production.

We selected the three sets of parameters denoting by A , B and C for the PBH abundance f_{PBH} . In case A , f_{PBH} enhances to $\mathcal{O}(10^{-3})$, which is compatible with the upper limit of LIGO, as shown in Fig. 4. In case B , f_{PBH} falls into the allowed region of ultrashort timescale in OGLE data. For this case, we obtained the peak value of f_{PBH} as $\sim \mathcal{O}(10^{-2})$ at the mass scale $\sim \mathcal{O}(10^{-5})M_{\odot}$. For the parameter set C , at the mass scale $\sim \mathcal{O}(10^{-12})M_{\odot}$ the PBH forms by the abundance $f_{\text{PBH}} \sim 0.92$. This confirms that the PBH production can justify most of DM in the universe.

In addition, we investigated the production of induced GWs for all parameter sets listed in Table I. For the cases A and B , the peaks of GWs energy density parameter are located near 10^{-10}Hz and 10^{-7}Hz , respectively, which can be tested by the SKA observation. For the parameter set C , the peak of Ω_{GW} falls into mHz band and this can be explored by the observations of LISA, Taiji, and TianQin. Our numerical calculations indicate that the GWs energy density parameter behaves like a power-law function $\Omega_{\text{GW}} \sim (f/f_c)^n$. We obtained $\Omega_{\text{GW}} \sim f^{2.1}$ for $f < f_c = 3.62 \times 10^{-3}\text{Hz}$ and $\Omega_{\text{GW}} \sim f^{-3.36}$ for $f > f_c$. In the infrared limit $f \ll f_c$, the power index has the logarithmic form $n = 3 - 2/\ln(f_c/f)$, which is in good agreement with the analytical result obtained in [89].

-
- [1] S. Hawking, Mon. Not. R. Astron. Soc. **152**, 75 (1971).
 - [2] B. J. Carr and S.W. Hawking, Mon. Not. R. Astron. Soc. **168**, 399 (1974).
 - [3] B. J. Carr, Astrophys. J. **201**, 1 (1975).
 - [4] Ya. B. Zel'dovich and I. D. Novikov, Sov. Astron. **10**, 602 (1967).
 - [5] B. P. Abbott et al. (LIGO Scientific Collaboration and Virgo Collaboration), Phys. Rev. Lett. **116**, 061102 (2016).
 - [6] B. P. Abbott et al. (LIGO Scientific Collaboration and Virgo Collaboration), Phys. Rev. Lett. **116**, 241103 (2016).

- [7] B. P. Abbott et al. (LIGO Scientific Collaboration and Virgo Collaboration), *Phys. Rev. Lett.* **116**, 221101 (2017).
- [8] B. P. Abbott et al. (LIGO Scientific Collaboration and Virgo Collaboration), *Astrophys. J.* **851**, L35 (2017).
- [9] B. P. Abbott et al. (LIGO Scientific Collaboration and Virgo Collaboration), *Phys. Rev. Lett.* **119**, 141101 (2017).
- [10] S. Bird, I. Cholis, J. B. Muñoz, Y. Ali-Haïmoud, M. Kamionkowski, E. D. Kovetz, A. Raccanelli, and A. G. Riess, *Phys. Rev. Lett.* **116**, 201301 (2016).
- [11] S. Clesse and J. Garc´ıa-Bellido, *Phys. Dark Universe* **15**, 142 (2017).
- [12] M. Sasaki, T. Suyama, T. Tanaka, and S. Yokoyama, *Phys. Rev. Lett.* **117**, 061101 (2016).
- [13] B. Carr, F. Kuhnel, and M. Sandstad, *Phys. Rev. D* **94**, 083504 (2016).
- [14] H. Niikura, M. Takada, S. Yokoyama, T. Sumi, and S. Masaki, *Phys. Rev. D* **99**, 083503 (2019).
- [15] P. W. Graham, S. Rajendran, and J. Varela, *Phys. Rev. D* **92**, 063007 (2015).
- [16] H. Niikura et al., *Nat. Astron.* **3**, 524 (2019).
- [17] R. G. Cai, S. Pi, S. J. Wang, and X. Y. Yang, *JCAP* **05**, 013 (2019).
- [18] G. Sato-Polito, E. D. Kovetz, and M. Kamionkowski, *Phys. Rev. D* **100**, 063521 (2019).
- [19] Y. Akrami et al. (Planck Collaboration), *A&A* **641**, A10 (2020).
- [20] K. Kohri and T. Terada, *Phys. Rev. D* **97**, 123532 (2018).
- [21] R. G. Cai, S. Pi, and M. Sasaki, *Phys. Rev. Lett.* **122**, 201101 (2019).
- [22] R. G. Cai, S. Pi, S. J. Wang, and X. Y. Yang, *JCAP* **05**, 013 (2019).
- [23] N. Bartolo, V. De Luca, G. Franciolini, A. Lewis, M. Peloso, and A. Riotto, *Phys. Rev. Lett.* **122**, 211301 (2019).
- [24] N. Bartolo, V. De Luca, G. Franciolini, M. Peloso, D. Racco, and A. Riotto, *Phys. Rev. D* **99**, 103521 (2019).
- [25] S. Wang, T. Terada, and K. Kohri, *Phys. Rev. D* **99**, 103531 (2019).
- [26] Y. F. Cai, C. Chen, X. Tong, D. G. Wang, and S. F. Yan, *Phys. Rev. D* **100**, 043518 (2019).
- [27] W. T. Xu, J. Liu, T. J. Gao, and Z. K. Guo, *Phys. Rev. D* **101**, 023505 (2020).
- [28] Y. Lu, Y. Gong, Z. Yi, and F. Zhang, *JCAP* **12**, 031 (2019).
- [29] F. Hajkarim and J. Schaffner-Bielich, *Phys. Rev. D* **101**, 043522 (2020).
- [30] Y. F. Cai, X. Tong, D. G. Wang, and S. F. Yan, *Phys. Rev. Lett.* **121**, 081306 (2018).

- [31] G. Ballesteros, J. B. Jim ´enez, and M. Pieroni, JCAP **06**, 016 (2019).
- [32] A. Y. Kamenshchik, A. Tronconi, T. Vardanyan, and G. Venturi, Phys. Lett. B **791**, 201 (2019).
- [33] K. Inomata, M. Kawasaki, K. Mukaida, and T. T. Yanagida, Phys. Rev. D **97**, 043514 (2018).
- [34] H. Motohashi and W. Hu, Phys. Rev. D **96**, 063503 (2017).
- [35] C. Germani and T. Prokopec, Phys. Dark Univ. **18**, 6 (2017).
- [36] H. Di and Y. Gong, JCAP **07**, 007 (2018).
- [37] J. M. Ezquiaga, J. Garc ´ia-Bellido, and E. R. Morales, Phys. Lett. B **776**, 345 (2018).
- [38] G. Ballesteros and M. Taoso, Phys. Rev. D **97**, 023501 (2018).
- [39] I. Dalianis, A. Kehagias, and G. Tringas, JCAP **01**, 037 (2019).
- [40] C. Chen and Y. F. Cai, JCAP **10**, 068 (2019).
- [41] O. Ozsoy, S. Parameswaran, G. Tasinato, and I. Zavala, JCAP **07**, 005 (2018).
- [42] Y. Tada and S. Yokoyama, Phys. Rev. D **100**, 023537 (2019).
- [43] J. Liu, Z. K. Guo, and R. G. Cai, Phys. Rev. D **101**, 023513 (2020).
- [44] J. Garc ´ia-Bellido and E. R. Morales, Phys. Dark Univ. **18**, 47 (2017).
- [45] S. S. Mishra and V. Sahni, JCAP **04**, 007 (2020).
- [46] T. Kobayashi, M. Yamaguchi, J. Yokoyama, Phys. Rev. Lett. **105**, 231302 (2010).
- [47] G. W. Horndeski, Int. J. Theor. Phys. **10**, 363 (1974).
- [48] S. Hirano, T. Kobayashi and S. Yokoyama, Phys. Rev. D **94**, 103515 (2016).
- [49] J. Ohashi and S. Tsujikawa, JCAP **10**, 035 (2012).
- [50] A. De Felice, S. Tsujikawa, Phys. Rev. D **84**, 083504 (2011).
- [51] A. De Felice, S. Tsujikawa, J. Elliston, R. Tavakol, JCAP **08**, 021 (2011).
- [52] Z. Teimoori and K. Karami, Astrophys. J. **864**, 41 (2018).
- [53] K. Inomata and T. Nakama, Phys. Rev. D **99**, 043511 (2019).
- [54] K. Inomata, M. Kawasaki, and Y. Tada, Phys. Rev. D **94**, 043527 (2016).
- [55] D. J. Fixsen, E. S. Cheng, J. M. Gales, J. C. Mather, R. A. Shafer, and E. L. Wright, Astrophys. J. **473**, 576 (1996).
- [56] C. Fu, P. Wu, and H. Yu, Phys. Rev. D **100**, 063532 (2019).
- [57] M. Sasaki, T. Suyama, T. Tanaka and S. Yokoyama, Class. Quantum Grav. **35**, 063001 (2018).
- [58] D.S. Salopek, J.R. Bond and J.M. Bardeen, Phys. Rev. D **40**, 1753 (1989).
- [59] V.F. Mukhanov and M.I. Zelnikov, Phys. Lett. B **263**, 169 (1991).

- [60] A.A. Starobinsky, JETP Lett. **55**, 489 (1992)
- [61] J. Garcia-Bellido, A. Linde and D. Wands, Phys. Rev. D **54**, 6040 (1996).
- [62] L. Randall, N. Sikjadic and A. Guth, Phys. Lett. B **472**, 377 (1996).
- [63] P. Ivanov, P. Nasselsky and I.D. Novikov, Phys. Rev. D **50**, 7173 (1994)
- [64] P. Ivanov, Phys. Rev. D **57**, 7145 (1998)
- [65] K. Inomata, M. Kawasaki, K. Mukaida, Y. Tada and T. T. Yanagida, Phys. Rev. D **96**, no. 4, 043504 (2017)
- [66] S. Young, C. T. Byrnes, and M. Sasaki, JCAP **07**, 045 (2014).
- [67] T Harada, C.-M. Yoo, and K. Kohri, Phys. Rev. D **88**, 084051 (2013).
- [68] I. Musco and J. C. Miller, Class. Quant. Grav. **30**, 145009 (2013).
- [69] C. Germani and I. Musco, Phys. Rev. Lett. **122**, no. 14, 141302 (2019)
- [70] M. Shibata and M. Sasaki, Phys. Rev. D **60** (1999) 084002.
- [71] A. G. Polnarev and I. Musco, Class. Quant. Grav. **24**, 1405 (2007).
- [72] I. Musco, J. C. Miller and A. G. Polnarev, Class. Quant. Grav. **26**, 235001 (2009).
- [73] Y. Ali-Haïmoud, E. D. Kovetz, and M. Kamionkowski, Phys. Rev. D **96**, 123523 (2017).
- [74] B. J. Carr, K. Kohri, Y. Sendouda, and J. Yokoyama, Phys. Rev. D **81**, 104019 (2010)
- [75] A. Barnacka, J. F. Glicenstein, and R. Moderski, Phys. Rev. D **86**, 043001 (2012).
- [76] K. Griest, A. M. Cieplak, and M. J. Lehner, Phys. Rev. Lett. **111**, 181302 (2013).
- [77] P. Tisserand et al. (EROS-2 Collaboration), Astron. Astrophys. **469**, 387 (2007).
- [78] Y. Ali-Haïmoud and M. Kamionkowski, Phys. Rev. D **95**, 043534 (2017).
- [79] V. Poulin, P. D. Serpico, F. Calore, S. Clesse, and K. Kohri, Phys. Rev. D **96**, 083524 (2017).
- [80] R. D. Ferdman et al., Class. Quant. Grav. **27**, 084014 (2010).
- [81] G. Hobbs et al., Class. Quant. Grav. **27**, 084013 (2010).
- [82] M. A. McLaughlin, Class. Quant. Grav. **30**, 224008 (2013).
- [83] G. Hobbs, Class. Quant. Grav. **30**, 224007 (2013).
- [84] P. Amaro-Seoane et al. (LISA Collaboration), arXiv:1702.00786.
- [85] K. N. Ananda, C. Clarkson, and D. Wands, Phys. Rev. D **75**, 123518 (2007).
- [86] D. Baumann, P. J. Steinhardt, K. Takahashi and K. Ichiki, Phys. Rev. D **76**, 084019 (2007).
- [87] C. Fu, P. Wu, and H. Yu, Phys. Rev. D **101**, 023529 (2020).
- [88] S. Kuroyanagi, T. Chiba, and T. Takahashi, JCAP **11**, 038 (2018).
- [89] C. Yuan, Z. C. Chen, and Q. G. Huang, Phys. Rev. D **101**, 043019 (2020).

- [90] C. J. Moore, R. H. Cole, and C. P. L. Berry, *Class. Quant. Grav.* **32**, 015014 (2015).
- [91] G. M. Harry (LIGO Scientific Collaboration), *Class. Quant. Grav.* **27**, 084006 (2010).
- [92] J. Aasi et al. (LIGO Scientific Collaboration), *Class. Quant. Grav.* **32**, 074001 (2015).
- [93] K. Danzmann, *Class. Quant. Grav.* **14**, 1399 (1997).
- [94] W.-R. Hu and Y.-L. Wu, *Natl. Sci. Rev.* **4**, 685 (2017).
- [95] J. Luo et al. (TianQin Collaboration), *Class. Quant. Grav.* **33**, 035010 (2016).